Review Article | Cardiovascular Imaging

eISSN 2005-8330
https://doi.org/10.3348/kjr.2020.1507
Korean J Radiol 2021;22(12):1946-1963

Korean Journal of Radiology
KJR

Tricuspid Valve Imaging and Right Ventricular Function Analysis Using Cardiac CT and MRI

Yura Ahn, Hyun Jung Koo, Joon-Won Kang, Dong Hyun Yang

All authors: Department of Radiology and Research Institute of Radiology, Cardiac Imaging Center, University of Ulsan College of Medicine, Asan Medical Center, Seoul, Korea

Cardiac computed tomography (CT) and cardiac magnetic resonance imaging (CMR) can reveal the detailed anatomy and function of the tricuspid valve and right ventricle (RV). Quantification of tricuspid regurgitation (TR) and analysis of RV function have prognostic implications. With the recently available transcatheter treatment options for diseases of the tricuspid valve, evaluation of the tricuspid valve using CT and CMR has become important in terms of patient selection and procedural guidance. Moreover, CT enables post-procedural investigation of the causes of valve dysfunction, such as pannus or thrombus. This review describes the anatomy of the tricuspid valve and CT and CMR imaging protocols for right heart evaluation, including RV function and TR analyses. We also demonstrate the pre-procedural planning for transcatheter treatment of TR and imaging of postoperative complications using CT.

Keywords: *Tricuspid valve; Tricuspid regurgitation; Transcatheter tricuspid valve repair; Cardiac computed tomography; Cardiac magnetic resonance imaging*

INTRODUCTION

The imaging of tricuspid valve disease has been investigated less than that of left-sided valve disease, largely because of the late onset of symptoms and the difficulty in image acquisition. Interest in the tricuspid valve has increased over the past two decades after recognition of the prognostic implications of functional tricuspid regurgitation (TR) [1,2] and the introduction of the transcatheter approach to the tricuspid valve. The role of imaging modalities in assessing the extent of TR and selecting appropriate candidates for transcatheter treatment has become increasingly important.

Right ventricle (RV) function analysis plays an important role in evaluating the pathogenesis, diagnosis, and prognosis of cardiopulmonary diseases, including congestive heart failure, pulmonary hypertension, and pulmonary embolism [3,4]. Although transthoracic echocardiography (TTE) is a first-line imaging modality for analyzing ventricular function, it is limited because the RV has a thin wall with heavy trabeculation, which makes it difficult to delineate. Cardiac magnetic resonance imaging (CMR) is considered the gold standard for volumetric quantification of the RV, as it provides excellent endocardial definition, and enables quantitative measurement of TR using phase-contrast images.

Cardiac computed tomography (CT) and CMR have enabled a more comprehensive understanding of the tricuspid valve. In this article, we review the anatomy of the tricuspid valve and CT and CMR protocols for the assessment of the right heart, illustrating methods for RV function and TR analyses using cardiac CT and CMR. Additionally, we demonstrate the use of cardiac CT in the planning of transcatheter treatment of TR and the evaluation of postoperative complications.

Received: December 30, 2020 **Revised:** May 25, 2021
Accepted: May 27, 2021

Corresponding author: Hyun Jung Koo, MD, PhD, Department of Radiology and Research Institute of Radiology, Cardiac Imaging Center, Asan Medical Center, University of Ulsan College of Medicine, 88 Olympic-ro 43-gil, Songpa-gu, Seoul 05505, Korea.
• E-mail: radkoo@amc.seoul.kr

Tricuspid Valve Anatomy

Tricuspid Valve Leaflets and Commissures

The tricuspid valve is a right atrioventricular valve with

Korean Journal of Radiology
KJR

a complex anatomy, which consists of four components: three leaflets (anterior, septal, and posterior) (Fig. 1), the fibrous annulus, the chordae tendineae, and papillary muscles. The three leaflets of the tricuspid valve vary in size and mobility; the anterior leaflet is the largest, with the longest radial length and the greatest motion. Conversely, the posterior leaflet is the smallest and has less functional significance; therefore, it can sometimes be surgically removed without impairment of valve function [5]. The septal leaflet has the shortest radial length and lowest mobility. The commissure between the anterior and septal leaflets is the longest commissure and lies on the membranous septum that divides the atrioventricular and interventricular portions [6]. The non-coronary sinus of Valsalva is located adjacent to this anteroseptal commissure and can be injured during transcatheter intervention [7]. The commissure between the septal and posterior leaflets is adjacent to the entrance of the coronary sinus into the right atrium.

Tricuspid Annulus

The tricuspid annulus is a D-shaped saddle-like non-planar structure consisting of two distinct structures: a larger C-shaped segment (the posterolateral segment of the annulus corresponding to the right atrium and RV free wall) and a relatively straight segment (the anterior-septal segment of the annulus corresponding to the septal leaflet and ventricular septum). The tricuspid annulus is a dynamic structure, and in healthy people, its orifice area undergoes changes of up to 29% from diastole to systole (Fig. 2) [8]. Its size is largest in late diastole after atrial contraction [9].

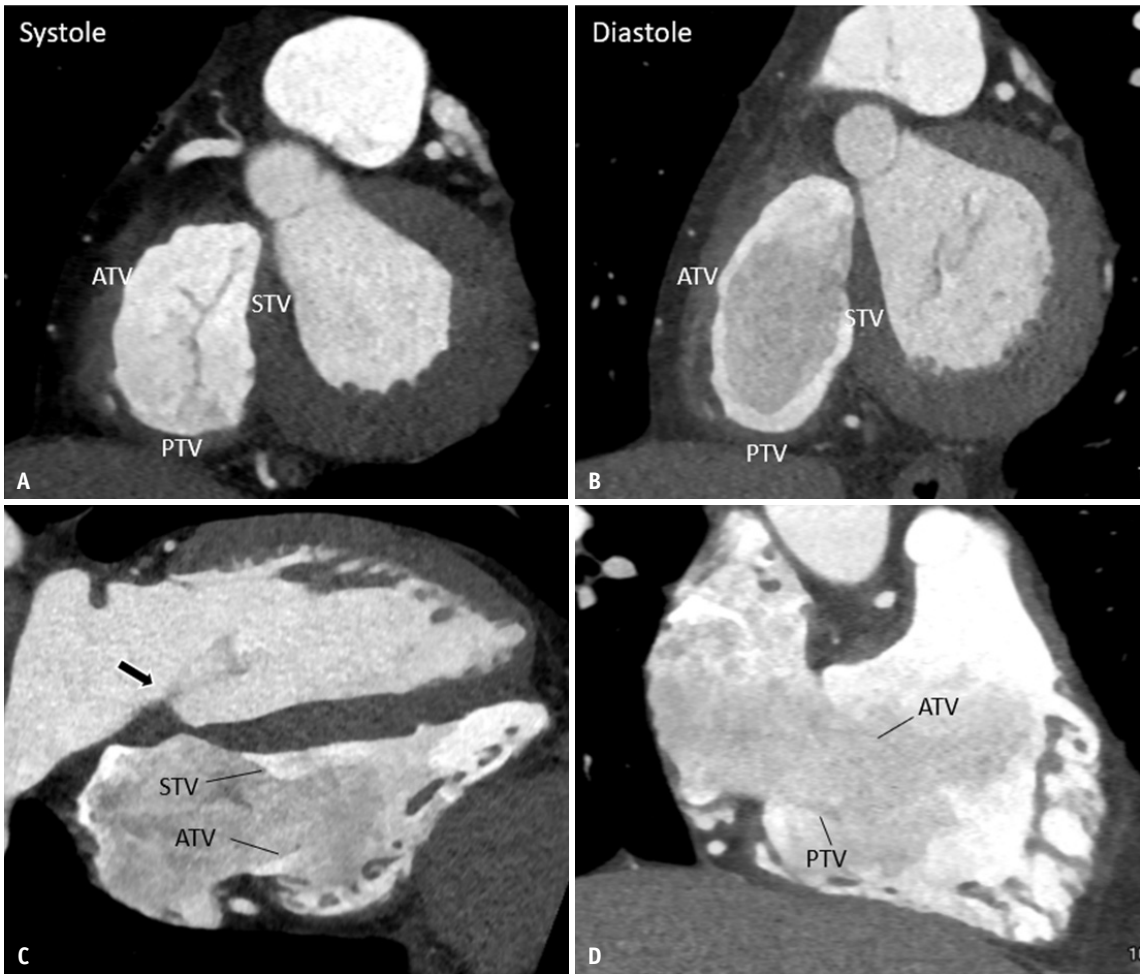

Fig. 1. CT images of the tricuspid valve.
A, B. Short-axis views toward the tricuspid valve at the right ventricular side in the systolic (35% of R-R interval) and diastolic (70% of R-R interval) phases. **C.** Septal and anterior tricuspid leaflets on the long-axis four-chamber view. The tricuspid annulus is located more apically than the mitral valve annulus (arrow). **D.** Posterior and anterior leaflets are visualized on the long-axis right two-chamber view. ATV = anterior tricuspid valve leaflet, PTV = posterior tricuspid valve leaflet, STV = septal tricuspid valve leaflet

https://doi.org/10.3348/kjr.2020.1507

Subvalvular Apparatus

Two papillary muscles and a third variable papillary muscle provides tense support to the tricuspid valve leaflets (Fig. 3). Of the two papillary muscles, the anterior papillary muscle arising from the anterior RV wall is larger and provides chordal support to the anterior and posterior leaflets. The moderator band extends from the trabecular septo-marginalis, arising from the interventricular septum to the base of the anterior papillary muscle. These connections form a U-shaped complex structure, dividing the inflow and outflow portions of the RV (Fig. 3) [10]. The posterior papillary muscles arising from the inferior wall provide chordal support to the posterior and septal leaflets. The septal papillary muscle is small and is present in multiples, or may even be absent in the normal population. It arises from the conus or RV septal wall and connects the chordae to the anterior and septal leaflets. Because the two leaflets (septal and anterior) are connected to the RV septal wall, and two leaflets (anterior and posterior) are also connected to the anterior RV wall via the anterior papillary muscle, displacement of the RV septum or anterior wall affects the coaptation of the leaflets. Among the three leaflets, the septal leaflet has a characteristic chordal attachment, with direct attachment of the chorda to the septum or main medial papillary muscle, which in turn inserts into the trabecular septo-marginalis; this can contribute to tethering of leaflets when the dilated RV displaces the papillary muscle [7]. Furthermore, chordae tendinae can be an obstacle when attempting the transcatheter approach to investigate the tricuspid valve.

Adjacent Anatomy

The septal atrioventricular junction is a central structure of the heart where the septal components of the atria and ventricles connect with the aortic, mitral, and tricuspid valves. This region includes the muscular atrioventricular septum, membranous septum, central fibrous body, Koch triangle, and the base of the interventricular septum (Fig. 4)

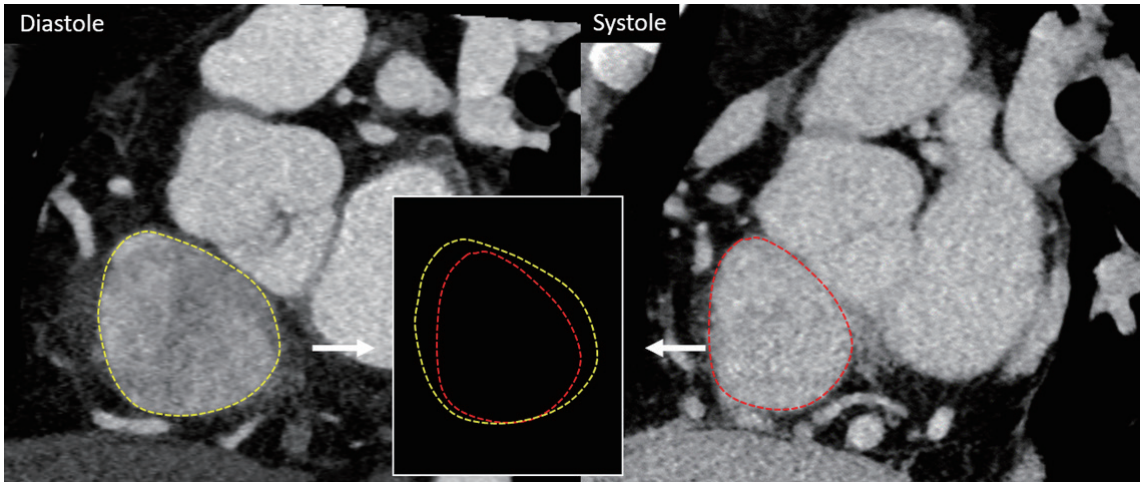

Fig. 2. Change in the tricuspid annulus shape during the cardiac phases. The area and perimeter of the tricuspid annulus are increased to the maximum size during diastole (yellow-dotted line). The diastolic phase image was obtained in the arterial phase by a bolus tracking method, 5–6 seconds after the ascending aorta reached 100 Hounsfield unit during a biphasic protocol. The tricuspid annulus size decreases during systole to the maximum size at end-systole (red-dotted line). The systolic phase image was obtained using a triphasic protocol.

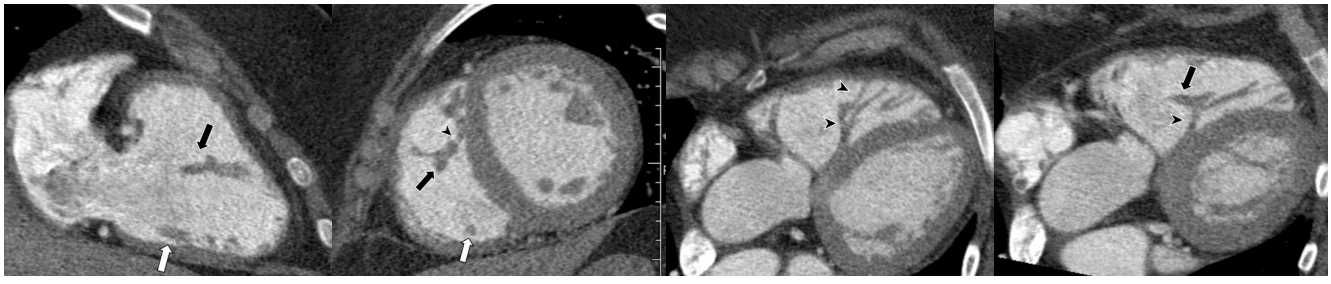

Fig. 3. Subvalvular apparatus. Anterior papillary muscle (black arrows) and posterior papillary muscle (white arrows) on a long-axis right two-chamber view, short-axis view, and five-chamber views. The moderator band (black arrowheads) originates from the trabecular septo-marginalis and joins the base of the anterior papillary muscle, crossing the right ventricular cavity. This anatomy forms the U-shaped structure.

https://doi.org/10.3348/kjr.2020.1507

Korean Journal of Radiology
KJR

[11]. The septal leaflet of the tricuspid valve is hinged from the right side of the membranous septum and divides it into atrioventricular and interventricular components. The triangle of Koch is a part of the medial right atrial wall, which is located at the level of the inferior pyramidal space. It contains the atrioventricular node and is therefore an important site for catheter ablation [12].

Anatomic Considerations for Transcatheter Tricuspid Valve Therapy

There are several anatomic features that must be considered before transcatheter tricuspid valve therapy. First, the right coronary artery (RCA) courses adjacent to the tricuspid annulus on the anterolateral side of the annulus, which has the anatomic goal of annular reduction, and cardiogenic shock secondary to direct injury to the RCA can occur. Injury to the atrioventricular node located within the triangle of Koch, adjacent to the tricuspid annulus, can also cause conduction disturbances. In addition, the fibrous annulus makes it difficult to anchor the device effectively. Furthermore, the transcatheter approach is difficult in a highly dilated annulus without calcification, as may be present in patients with the most severe TR. Finally, patients with pacemakers or cardiac implantable electronic devices *in situ* can present limitations in the insertion of devices [13].

Types of Tricuspid Regurgitation

TR can be divided into two types, primary and secondary, according to their pathophysiology. Primary TR results from a primitive lesion in the tricuspid valve, which may be the result of a congenital anomaly (e.g., Ebstein's

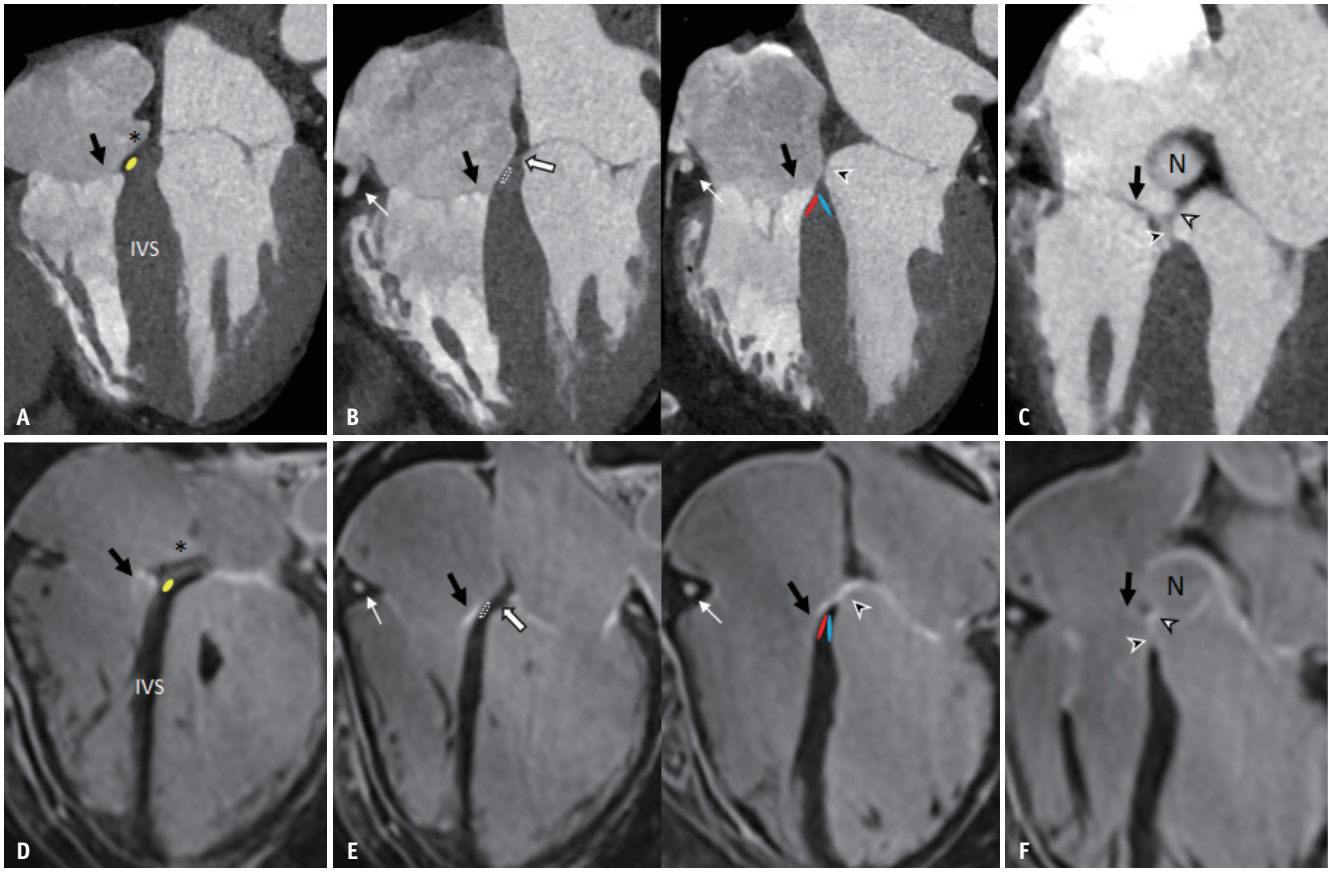

Fig. 4. Relationship of the septal leaflet of the TV with the atrioventricular junction and conduction axis on cardiac CT (A-C) and MRI (D-F, contrast-enhanced T1-weighted fast low angle shot inversion recovery sequence).
A, D. The atrioventricular node (yellow circle) can be found at the ostium of the coronary sinus (asterisks) level, at the level of septal leaflet of the TV (black arrows) hinges. **B, E.** Superior level of **(A)**; the bundle of His (white-dotted circle) exits from the atrioventricular node and passes the muscular atrioventricular septum (thick white arrows) level. The membranous septum (arrowheads) is located above the muscular atrioventricular septum, where the septal leaflet of the TV (black arrows) hinges. The bundle of His is divided into the right bundle branch (red circle) and left bundle branch (blue circle) at the crest of the IVS. The right coronary artery (thin white arrows) courses along the tricuspid annulus. **C, F.** The septal leaflet of the TV (black arrows) divides the membranous septum in the interventricular (black arrowheads) and atrioventricular membranous septum (white arrowheads). IVS = interventricular septum, N = non-coronary sinus of Valsalva, TV = tricuspid valve

https://doi.org/10.3348/kjr.2020.1507

anomaly) or an acquired disease (e.g., rheumatic disease, endocarditis, or myxomatous degeneration). Primary TR is rare and should be distinguished from secondary TR for appropriate clinical management [7]. Secondary (functional) TR is the most common form, resulting from morphological abnormalities in the RV and tricuspid apparatus: tethering or tenting of the leaflet, tricuspid annular dilatation, or malcoaptation caused by RV dilatation and dysfunction [14]. The underlying disease can be further classified into four categories as follows [7]: 1) left-sided heart disease, such as mitral valve disease or LV dysfunction, 2) pulmonary arterial hypertension, 3) conditions resulting from RV dysfunction, such as myocardial infarction/ischemia, and 4) idiopathic TR with no detectable cause.

CT Imaging Techniques and Analyses

Cardiac CT Protocol for Right Heart Evaluation

Clear visualization of the right atrioventricular junction is challenging. The contrast media injection protocol for visualization of the right heart structures on cardiac CT differs from that used for left heart visualization. In conventional routine coronary CT angiography using the bolus tracking method, scanning is started 5–6 seconds after the ascending aorta reaches 100–140 Hounsfield unit (HU), which causes heterogeneous attenuation of the right-side heart with a mix of contrast agent and blood [15]. Therefore, a modified protocol is needed, which involves using a 50% dose of contrast media (1:1 mixture of contrast media and saline) and saline chasing; and provides homogeneous attenuation of the RV cavity and outlet [5]. In our hospital, RV imaging is performed using a triphasic protocol that involves the injection of 60–65 mL contrast media, 20 mL of 70:30 saline-contrast mixture, and 40 mL saline chaser. However, this is sometimes insufficient for evaluation of the RV inlet and tricuspid valve because of inhomogeneous enhancement of the right atrium, and streak artifacts when contrast media in the superior vena cava mixes with unenhanced blood from the inferior vena cava [5]. To prevent this problem, a semi-invasive technique that simultaneously injects contrast agents via both the femoral and antecubital veins has been suggested [16]. This is an ideal method, but due to its invasiveness, the biphasic or triphasic protocol is generally used [17,18]. For function analysis with electrocardiography (ECG)-gated cardiac CT, multiphase data with a maximum 1.5-mm slice thickness reconstructed for at least 10 phases of the cardiac cycle (0%–90% of R-R interval) are required. A relatively high radiation dose is inevitable during multiphase cardiac-gated acquisition for the evaluation of ventricular function or dynamic motion of the heart valves. To reduce this radiation dose, ECG-controlled tube current modulation or wide-detector CT are options that are worthy of consideration [19,20]. Low-dose scanning with iterative reconstruction is another option for obtaining multiphase data with reduced radiation doses [21,22].

CT Image Reconstruction

To measure the tricuspid annulus on cardiac CT, it is recommended to use a reconstructed short-axis image with manual selection of the level of the plane at an annulus level on four-chamber and two-chamber images acquired at end-diastole (Fig. 5). The normal maximum annulus diameter, circumference, and area are 3.1 ± 0.4 cm, 11.9 ± 0.9 cm, and 11.3 ± 1.8 cm^2, respectively, on the four-chamber view of two-dimensional (2D) echocardiography [23,24], and 3.0–3.5 cm on the short-axis CT image [18]. In functional TR, which is characterized by a dilated annulus (> 40 mm) [25], the annulus dilates along the RV free wall, and the shape becomes more circular and flatter (Fig. 6) [26].

The four-chamber view of cardiac CT allows delineation of the location of the tricuspid leaflets and the three commissures. The septal leaflet directly arises from the medial side of the tricuspid annulus, above the interventricular septum, and ≤ 10 mm apical to the septal insertion of the anterior leaflet of the mitral valve (Fig. 1).

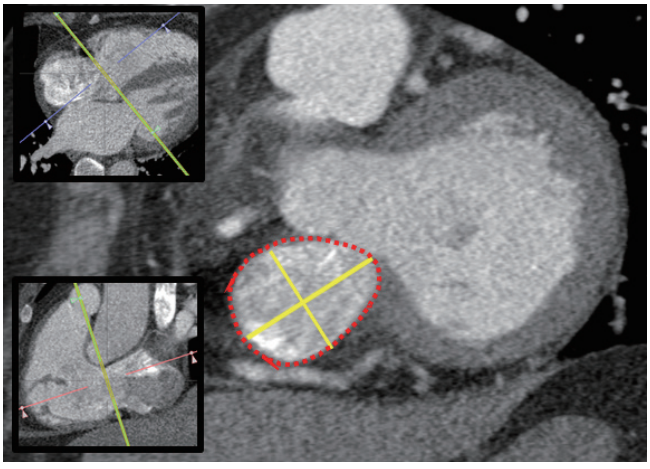

Fig. 5. Measurement of the tricuspid annulus on cardiac CT.
The perimeter (red-dotted line) and diameters (yellow lines) are measured on a reconstructed short-axis view by manually adjusting the plane level at the tricuspid annulus on the long-axis four-chamber (top box) and the long-axis two-chamber views (bottom box).

https://doi.org/10.3348/kjr.2020.1507

Korean Journal of Radiology
KJR

The muscular atrioventricular septum is located in the difference in the level of attachment of the tricuspid and mitral valves. The coaptation of leaflets occurs at the level of the annulus or just below the annulus, with a coaptation length of 5–10 mm [14]. The anterior and posterior tricuspid leaflets can be visualized on the right heart two-chamber view. The planning of transcatheter tricuspid valve therapy is based on four- and two-chamber CT views, and is discussed later in this review.

The normal RV free wall thickness is < 4 mm in a four-chamber view during diastole [27]. Chronic pressure overload in congenital heart disease, pulmonary hypertension, pulmonary valve stenosis, or RV outflow tract obstruction, causes RV hypertrophy. Because RV hypertrophy gradually progresses, it can help distinguish acute from chronic pulmonary embolism [28].

Right Ventricular Function Analysis Using CT

Cardiac CT has good accuracy and reproducibility for RV function analysis when compared to CMR as a reference method [4]. The advantages and disadvantages of cardiac CT and CMR are summarized in Table 1, and the normal RV parameters are summarized in Table 2 [29,30].

Table 2. Reference Values for Right Heart Function [29,30]

	CT	CMR
RV free wall, mm	< 4	
RV EDVI, mL/m^2		
Male	96 ± 15	91 ± 15
Female	88 ± 12	80 ± 16
RV ESVI, mL/m^2		
Male	42 ± 19	39 ± 10
Female	36 ± 15	32 ± 10
RV EF, %		
Male	58 ± 16	62 ± 5
Female	61 ± 14	61 ± 5

Parameters are described as mean ± standard deviation. CMR = cardiac magnetic resonance imaging, EDVI = end-diastolic volume index, EF = ejection fraction, ESVI = end-systolic volume index, RV = right ventricle

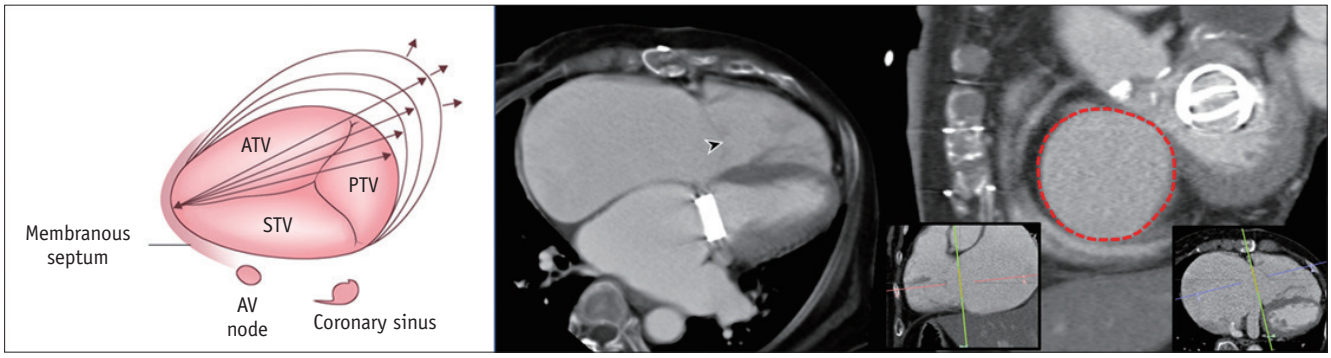

Fig. 6. Change in the tricuspid annulus in functional TR. Normally, the tricuspid annulus is a non-planar saddle-like stricture. As the right heart function deteriorates, the annulus dilates toward the anteroposterior direction, and the shape becomes more planar and circular (illustration). Two CT images of a 77-year-old female who underwent mitral valve replacement and had functional TR with right heart enlargement. The coaptation defect of the tricuspid valve occurs during the systolic phase (arrowhead). The tricuspid annulus is large and circular on the reconstructed short-axis view. ATV = anterior tricuspid valve leaflet, AV = atrioventricular, PTV = posterior tricuspid valve leaflet, STV = septal tricuspid valve leaflet, TR = tricuspid regurgitation

Table 1. Pros and Cons of Cardiac CT and MRI

	Cardiac CT	CMR
Pros	Good accuracy and reproducibility with CMR as the reference standard	The gold standard for RV volumetric quantification
	Useful in complex adult congenital heart disease patients with cardiac devices	High temporal resolution
	Short total scan time (time saving)	Excellent endocardial definition
		Regional wall motion abnormalities and tissue characterization
		Accurate and reproducible right heart volume measurement
		Quantitative measurement of TR with phase-contrast imaging
Cons	Limited tissue evaluation	High cost
	Ionizing radiation	Long total scan time
	Metallic artifacts	Relative contraindication if a metallic device is present (metallic artifacts exist even if CMR can be obtained)

CMR = cardiac magnetic resonance imaging, RV = right ventricle, TR = tricuspid regurgitation

https://doi.org/10.3348/kjr.2020.1507

The multiplanar reformatted image in the short-axis view was used for RV function analysis and mass measurement. The early signs of RV volume or pressure overload manifest as RV size alteration and can be assessed using the RV dimension and volume [31]. For volumetric measurement, the endocardial border is traced along the axis of the base to the apex. Both papillary muscles and trabeculations are generally incorporated into the RV cavity by manual contour tracing. These structures can be excluded from the volume quantification in a semiautomatic contouring method using attenuation threshold-based selection (Fig. 7). RV endocardial borders are segmented at end-diastole (the first image after the R-wave based on ECG, which gives the maximal cross-sectional area on short-axis cine images and with the largest RV blood volume) and end-systole (cardiac phase with minimal cross-sectional area at the same level) [32,33]. RV volumes were calculated by applying Simpson's method (an interpolated summation of stack of disks).

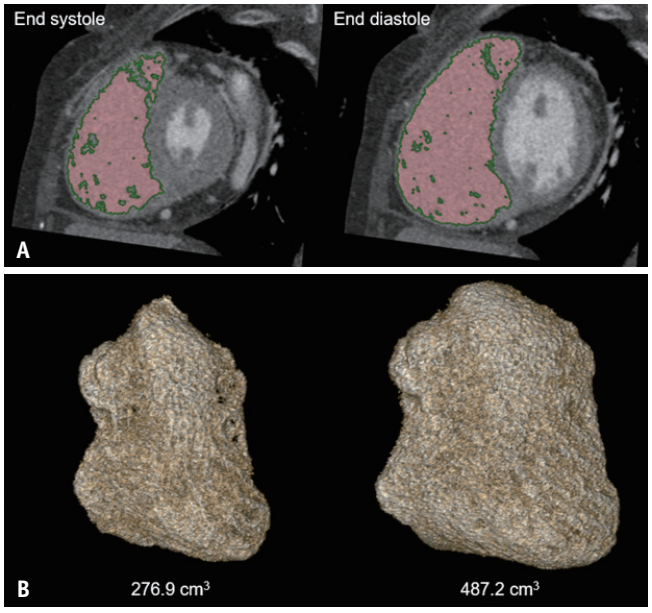

Fig. 7. Cardiac CT for RV function analysis.
A. Short-axis images with RV cavity selection using a semiautomatic contouring method with attenuation threshold-based selection in end-systole and end-diastole. The myocardial trabeculation and papillary muscles are excluded from the volume quantification. **B.** Volume-rendered images of the RV cavity can be generated to quantify the RV volume. RV = right ventricle

Assessment of TR with Cardiac CT

Compared to echocardiography and CMR, the quantification of TR using cardiac CT has not been systematically established. CT can be considered as an alternative modality only in patients with a suboptimal transthoracic echocardiographic window.

For the quantification of TR, tricuspid regurgitant volumes can be measured as the difference between the RV stroke volume and the LV stroke volume [34]. The anatomic regurgitant orifice area during mid-to-end-systole (20%–30% of the R-R interval), the tricuspid annulus area during mid-to-end-diastole (60%–80% of the R-R interval), and the tricuspid leaflet tethering area and height can be used to grade the severity of TR (Fig. 8) [35]. The regurgitant orifice area is the narrowest of the regurgitant orifice bordered by the tricuspid leaflet tips in the reformatted short-axis view. The tethering heights and area were measured on two- or four-chamber views by measuring the distance from the annular plane to the coaptation point and

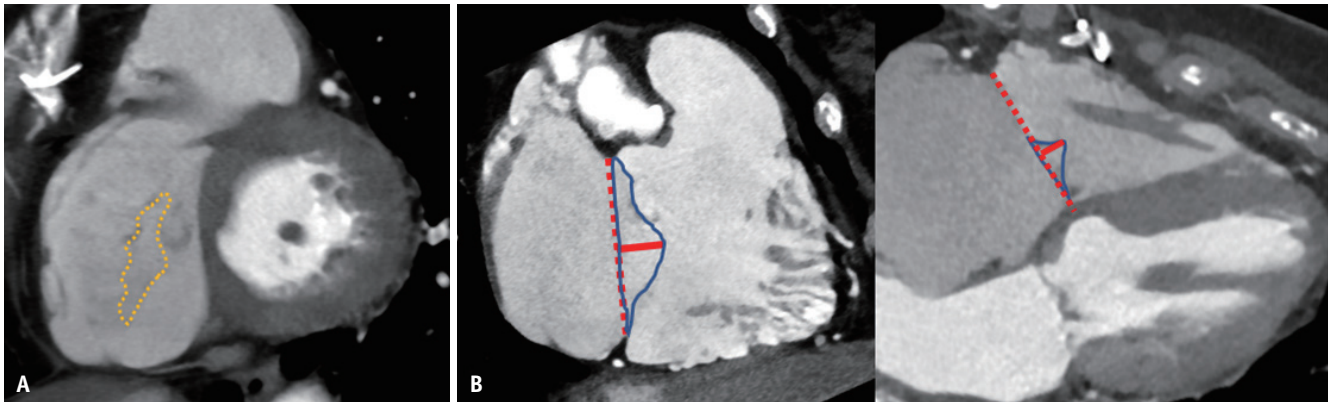

Fig. 8. An 63-year-old female with severe functional tricuspid regurgitation. Multiplanar reconstructed images were obtained at the end-systolic phase (30% of R-R interval).
A. The regurgitant orifice area is traced on the short-axis image with a yellow dashed line. **B.** The tricuspid tethering height (red solid line) and area (blue solid line) are measured on the long-axis right two-chamber and four-chamber images tracing the leaflets from the annular plane (red dotted line).

https://doi.org/10.3348/kjr.2020.1507

Korean Journal of Radiology
KJR

tracing the annular plane to the leaflets. The dimensions of the tricuspid annulus and tethering heights measured on CT correlated with the severity of TR and the prognosis of cardiovascular events in patients with moderate to severe TR [36,37]. Tethering height and area are predictors of recurrent TR in tricuspid annuloplasty [36,38], and tethering height measured on preoperative cardiac CT was an independent risk factor for postoperative recurrent TR, with a tethering height > 7.2 mm used as a cut-off value for recurrent TR after tricuspid annuloplasty (sensitivity, 72%; specificity, 100%) [36].

CMR Imaging Techniques and Analyses

CMR Protocol for Right Heart Evaluation

For volume and function analyses, the cine steady-state free-precession (SSFP) sequence with a temporal resolution < 45 ms/phase enabled the best assessment. The short-axis image should provide coverage from the base to the apex, with a slice thickness of 6–8 mm and a 2–4 mm interslice gap. The basal slice should be placed immediately on the myocardial side of the RV, and the atrial volume should be carefully removed from the basal slice at the end of systole [39]. In addition to the routinely acquired four-chamber RV long-axis view, other specialized views (RV two-chamber view, RV three-chamber view, and RV outflow tract view) should be obtained for RV and tricuspid valve evaluation, the relative orientations of which are shown in Figure 9.

Right Ventricular Function Analysis Using CMR

Similar to the function analysis on cardiac CT performed by tracing the endocardial margin, volumetric measurements were performed using Simpson's method. The end-systolic and end-diastolic phases were manually selected by identifying the minimum and maximum RV volumes. Post-processing software enables an accurate short-axis slice position with reference to the long-axis view and can be used to calculate the RV volume and mass (Fig. 10). The RV mass is obtained by tracing both the epicardial and endocardial borders, usually excluding the papillary muscles [17]. To interpret the CMR for RV functional assessment, qualitative assessment, including wall motion evaluation (pattern [global/septal/free wall] and extent [normal/hypokinetic/dyskinetic]), presence of hemodynamic

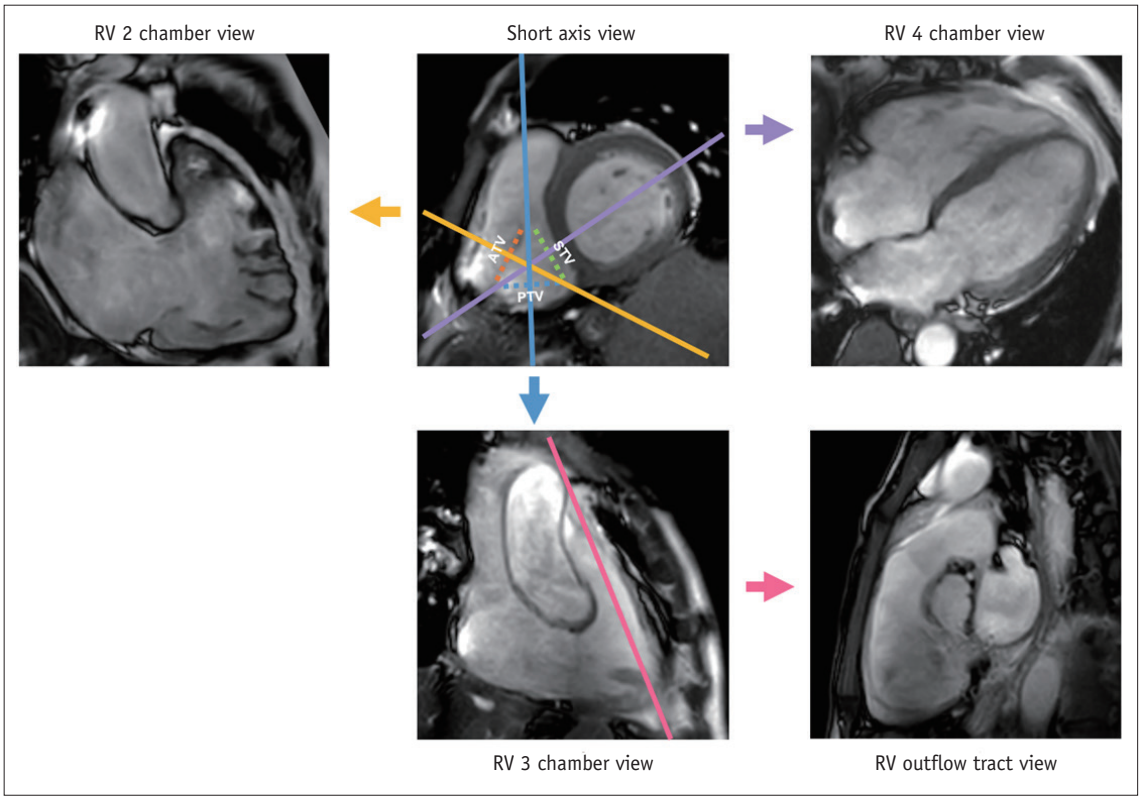

Fig. 9. Reconstructed views for right heart evaluation on cardiac magnetic resonance imaging. The right two-chamber, four-chamber, and three-chamber views can be obtained from the perpendicular plane to anterior septal, and the posterior tricuspid leaflets, respectively, on short-axis views. The RV outflow tract view is obtained from its perpendicular plane on the right three-chamber view. RV = right ventricle

https://doi.org/10.3348/kjr.2020.1507

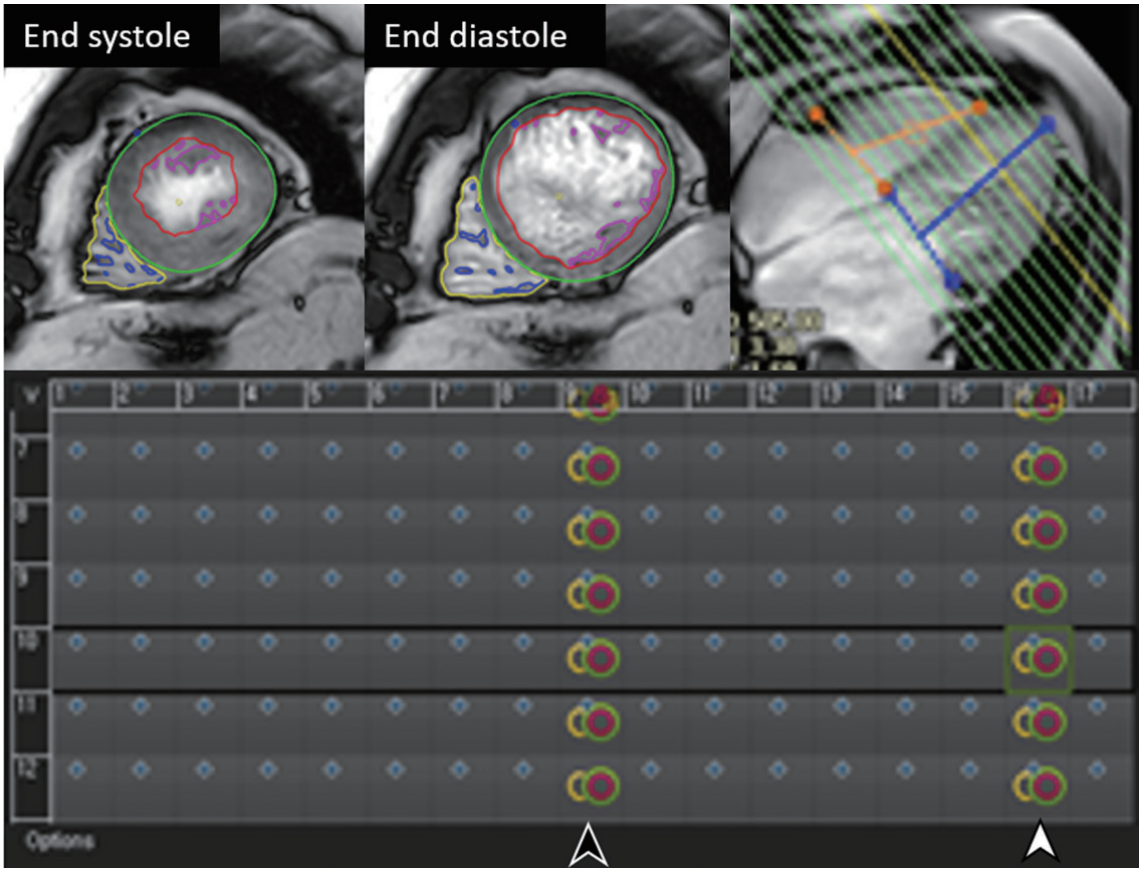

Fig. 10. Cardiac MR for RV function analysis. Short-axis cine images with RV manual contouring in end-systole (top left) and end-diastole (top middle). Each phase is manually selected when the RV shows minimum (black arrowhead) and maximum (white arrowhead) dimensions, respectively. Yellow lines indicate the endomyocardial RV border. Left ventricular endo- and epi-myocardial borders are drawn in red and green lines, respectively. Myocardial trabeculation and papillary muscles are excluded from the contouring. The volume was measured by Simpson's method using a stack of short-axis views. RV = right ventricle

interaction between RV and LV (e.g., the reaction of ventricular interdependence in constrictive pericarditis), RV wall thickness, and presence of RV dilatation can be evaluated. For quantitative assessment, the ejection fraction (%), end-diastolic, end-systolic, stroke volume (mL and mL/m^2 for a body surface area-indexed value), cardiac output (L/min), and cardiac index (L/min/m^2) of the RV can be measured [40].

Assessment of TR with CMR

Visualization of the RV and TR with good temporal and spatial resolution and without exposing the patient to ionizing radiation or intravenous contrast media is a major advantage of CMR. Reformatted multiplanar images enable the assessment and measurement of the tricuspid valve. On the cine SSFP image, TR can be qualitatively assessed by identifying the area of the signal drop due to turbulent flow and/or acceleration (Fig. 11). Spoiled gradient-recalled echo cine images, which have longer repetition and echo times, are also used for TR visualization when the flow void is not clearly shown on SSFP images [35]. However, this area of the signal void is affected by the echo time and windowing [41]. In addition, a higher magnetic field results in more prominent flow voids [35]. These factors should be considered before the assessment of TR to limit standardization difficulties. Although CMR enables the quantitative assessment of TR, not all MRI-specific cut-off values for the measurements have been established. The quantitative noninvasive imaging parameters that can be acquired using CMR and echocardiography are presented in Table 3 [5]. The cut-off values for severity grading were based mainly on the echocardiographic standards. For the TR fraction, recent guidelines suggest using the same severity cut-off used for mitral regurgitation (a regurgitant fraction ≤ 15% for mild TR, 16%–25% for moderate TR, 26%–48% for moderately severe TR, and > 48% for severe TR) [34].

The flow through the valve was measured using phase-contrast MRI. The regurgitant volume is indirectly measured

https://doi.org/10.3348/kjr.2020.1507

Korean Journal of Radiology
KJR

by subtracting the main pulmonary artery forward volume from the RV systolic volume calculated using a stack of short-axis images acquired using the method described above (Fig. 12). The TR volume can also be directly measured at the orthogonal plane of the tricuspid annulus in a velocity-encoding cine image, and this technique has shown considerable reproducibility [42].

Treatment Options for Tricuspid Valve Disease

Tricuspid valve surgery is a definitive therapy for patients with severe symptoms that are refractory to medical treatment [43]. The main purpose of surgery is to reduce the high RV afterload by correcting left-sided valve disease and correcting the dilated tricuspid annulus by annuloplasty (tricuspid valve repair) or tricuspid valve replacement when repair is unfeasible (e.g., marked leaflet tethering, complex primary TR, or severe tricuspid stenosis) [44]. Current guidelines recommend the timing of surgical treatment for severe functional TR at the same time as left-sided surgery or RV dysfunction [45]. Because evidence for the optimal timing of surgery is still insufficient, delaying surgery until after the development of overt RV dysfunction and end organ damage contributes to worse postoperative outcomes

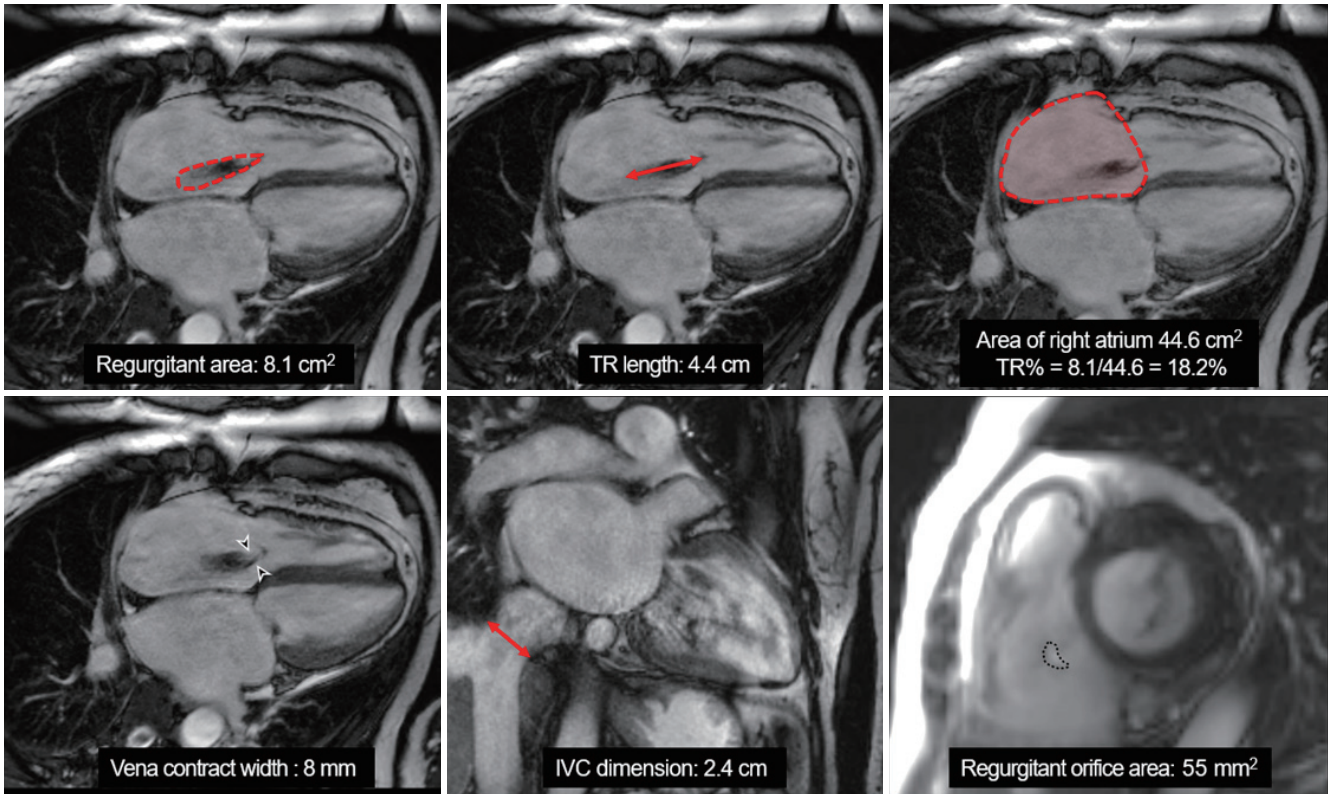

Fig. 11. Cardiac MR parameters for quantitative assessment of TR. A 67-year-old female with severe functional TR. On the cardiac cine image using a balanced steady-state free-precession sequence, the TR jet is represented as signal void. The regurgitant area, TR length, and TR (%) can be measured by delineating the signal void area. The vena contracta width is defined as the narrowest dimension of regurgitant flow adjacent to the regurgitant orifice, just before the flow expands. The dimension of the IVC is measured on the coronal cine image. The regurgitant orifice area was obtained on the short-axis cine image. IVC = inferior vena cava, TR = tricuspid regurgitation

Table 3. Cardiac MRI Parameters for Quantitative Assessment of TR

Severity	Regurgitant Area, cm^2	TR Length, cm	TR, %†	Vena Contracta Width, mm‡	Regurgitant Orifice Area, mm^2	Regurgitant Volume, mL*	RA, RV, IVC Dimensions, cm
Mild	< 5	2	20	Not defined	Not defined	Not defined	Nonspecific
Moderate	6–10	3–5	20–34	< 6.5	Not defined	Not defined	Nonspecific
Severe	> 10	> 5	> 35	> 7	> 40	> 45	IVC > 2

Adapted from Saremi et al. AJR Am J Roentgenol 2015;204:W531-W542, with permission of ARRS [5]. *RV systolic volume–main pulmonary artery forward volume, †Maximum regurgitant area divided by right atrial area, ‡Smallest regurgitant flow between convergence and expansion of flow. IVC = inferior vena cava, RA = right atrium, RV = right ventricle, TR = tricuspid regurgitation

https://doi.org/10.3348/kjr.2020.1507

Fig. 12. Calculation of tricuspid regurgitant volume. A 39-year-old male with severe functional tricuspid regurgitation. **A.** The through-plane phase-contrast image for pulmonary flow is obtained at the level just above the pulmonary valve, and the total forward flow (red-lined box) is measured by drawing a region of interest on the main pulmonary artery (red-lined area). **B.** The RV stroke volume (blue-lined box) is derived from both systolic and diastolic SAX stacks from the base to apex of the RV. The regurgitant volume was calculated by subtracting the pulmonary forward volume from the RV systolic volume as follows: 94.71–51.10 mL = 43.61 mL. BSA = body surface area, H = height, HR = heart rate, RV = right ventricle, RVCI = RV cardiac index, RVCO = RV cardiac output, RVEDV = RV end-diastolic volume, RVEF = RV ejection fraction, RVESV = RV end-systolic volume, RVSV = RV stroke volume, SAX = short axis

compared to those of the mitral or aortic valve [43]. For patients with such a high operative risk, a less invasive technique is of interest as a treatment option. Recently, various transcatheter tricuspid valve therapy techniques have been developed, which have shown promising results in the clinical evaluation stage [46]. Transcatheter tricuspid valve therapy is classified as transcatheter tricuspid valve repair, transcatheter tricuspid valve replacement, and heterotopic caval valve implantation.

Types of Device and CT Planning for Transcatheter Tricuspid Valve Therapy

Transcatheter tricuspid valve therapy can be categorized based on its anatomic therapeutic target (Fig. 13). Tricuspid valve repair can be classified as repair using a coaptation or annuloplasty device, heterotopic caval valve implantation (which is performed in the superior vena cava or inferior vena cava), and orthotopic transcatheter tricuspid valve replacement (Table 4) [13]. Cardiac CT has become an important imaging modality for pre-procedural evaluation, providing geometric information on the RV and tricuspid valve annulus (which is a non-planar structure making deployment and landing of the device hard), and clarifying the relationship between the RCA and tricuspid valve annulus, which is occasionally difficult to evaluate on echocardiography [47]. The measurement parameters obtained from cardiac CT for the planning of transcatheter tricuspid valve therapy are explained below and are shown in Figure 14.

1) Tricuspid annulus dimensions and distance between

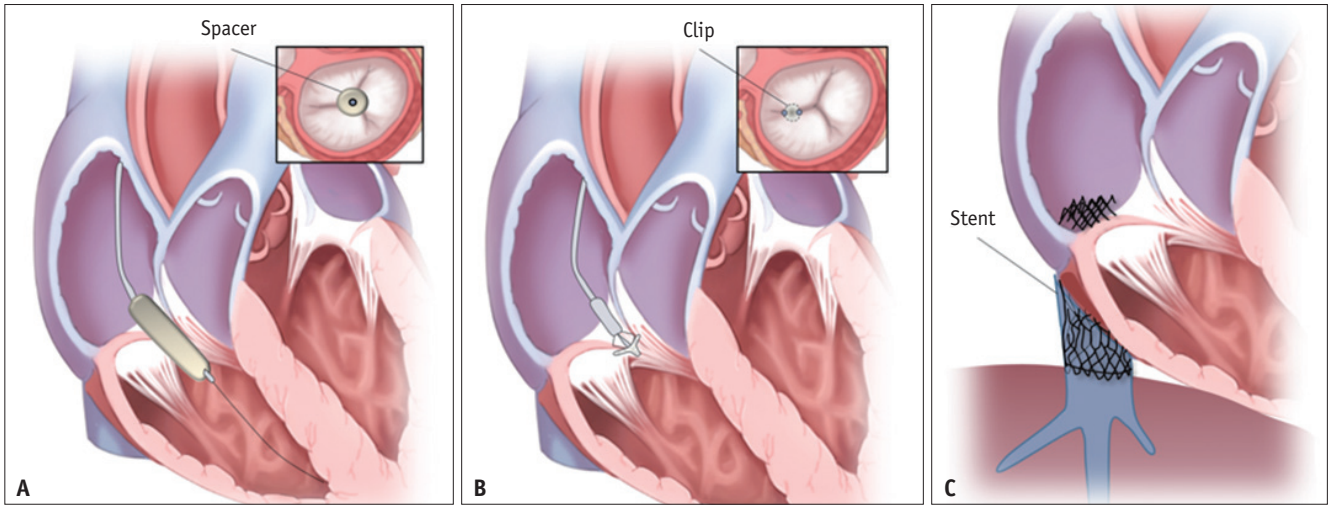

Fig. 13. Types of transcatheter therapy for tricuspid regurgitation.
A. A spacer device for improving leaflet coaptation and reducing the regurgitation orifice. **B.** A clipping device for direct suture annuloplasty. **C.** Heterotopic caval valve implanted in the inferior vena cava.

https://doi.org/10.3348/kjr.2020.1507

Korean Journal of Radiology
KJR

Table 4. Types of Transcatheter TV Therapy

Type	Mechanism	Anatomical Targets and Key Measures	Cardiac CT Images	Device	Ongoing Study
Annuloplasty	Divided into direct suture (Trialign, TriCinch, MIA) or ring (Cardioband, IRIS) annuloplasty device Reduce annular diameters by plication of tissue (direct suture) or bidirectional reshaping and reduction of annulus using attached ring (ring annuloplasty)	Course of RCA Distance between RCA and anterior/posterior TV leaflet insertion	Long-axis two-chamber and four-chamber views, volume-rendered images Long-axis four-chamber view, short axis of the TV	Trialign TriCinch Cardioband IRIS MIA	SCOUT II CE Mark study PREVENT TRI-REPAIR STTAR
Annular spacer	Polymer balloon is deployed at the TV to improve coaptation, with anchoring system implanted in the RV septal wall	Tricuspid annulus dimension Distance from the tricuspid annulus to the RV apex	Short axis of the TV Long-axis four-chamber view	Forma	SPACER
CAVI (heterotopic caval valve implantation)	Prevent caval backflow of TR and reduce symptoms and signs of RV failure (systemic venous congestion)	The dimension of IVC at the levels of the cavoatrial junction and first hepatic vein Distance from the IVC to the 1st hepatic vein	Transverse plane of cavoatrial junction Oblique sagittal plane of the IVC	TricValve® SapienXT	HOVER TRICAVAL
Valve replacement	Implantation of self-expandable bioprosthetic TV First reported in 2014	Tricuspid annulus dimension Course of RCA Distance from the tricuspid annulus to the RV apex The right internal jugular vein and SVC size RVOT evaluation	Short axis of the TV Long-axis two-chamber and four-chamber views, volume-rendered images Long-axis four-chamber view Double oblique transverse plane Sagittal oblique and short axis of RVOT	NaviGate	

Cardioband (Edwards Lifesciences), Forma (Edwards Lifesciences), IRIS (Millipede, Inc.), MIA (Micro Interventional Devices, Inc.), NaviGate (NaviGate Cardiac Structures, Inc.), SapienXT (Edwards Lifesciences), Trialign (Mitralign Inc.), TriCinch (4Tech Cardio Ltd.), TricValve® (P&F Products & Features). IVC = inferior vena cava, RCA = right coronary artery, RV = right ventricle, RVOT = RV outflow tract, SVC = superior vena cava, TR = tricuspid regurgitation, TV = tricuspid valve

the tricuspid valve annulus and the RV apex: in a spacer system, the anchoring system is first implanted into the RV septal free-wall groove. The spacer, a foam-filled polymer balloon, is located perpendicular to the tricuspid annular plane and reduces the coaptation gap. Therefore, a maximal distance between the tricuspid valve annulus and the RV apex is required. The dimensions (diameter, perimeter, and area) of the tricuspid valve on multiplanar images should be evaluated before implanting the device (which directly interacts with the tricuspid valve leaflet) and transcatheter tricuspid valve replacement.

2) Anatomic relationship with RCA: as the RCA often courses parallel to the tricuspid annulus during the direct tricuspid annuloplasty procedure or transcatheter tricuspid valve replacement, the RCA can impinge. CT provides an accurate measurement of the distance from the tricuspid valve annulus. Measurements were performed on short-axis and four-chamber views, and the clipping site was used for direct annuloplasty at the location of the anterior and posterior leaflets. The transcatheter procedure can be precluded by an unfavorable course (RCA ≤ 2 mm from the TA). [48]. If the RCA course is below or above the tricuspid annular level and not parallel to the annulus, thick-slabbed multiplanar images and volume-rendered images can be

 https://doi.org/10.3348/kjr.2020.1507

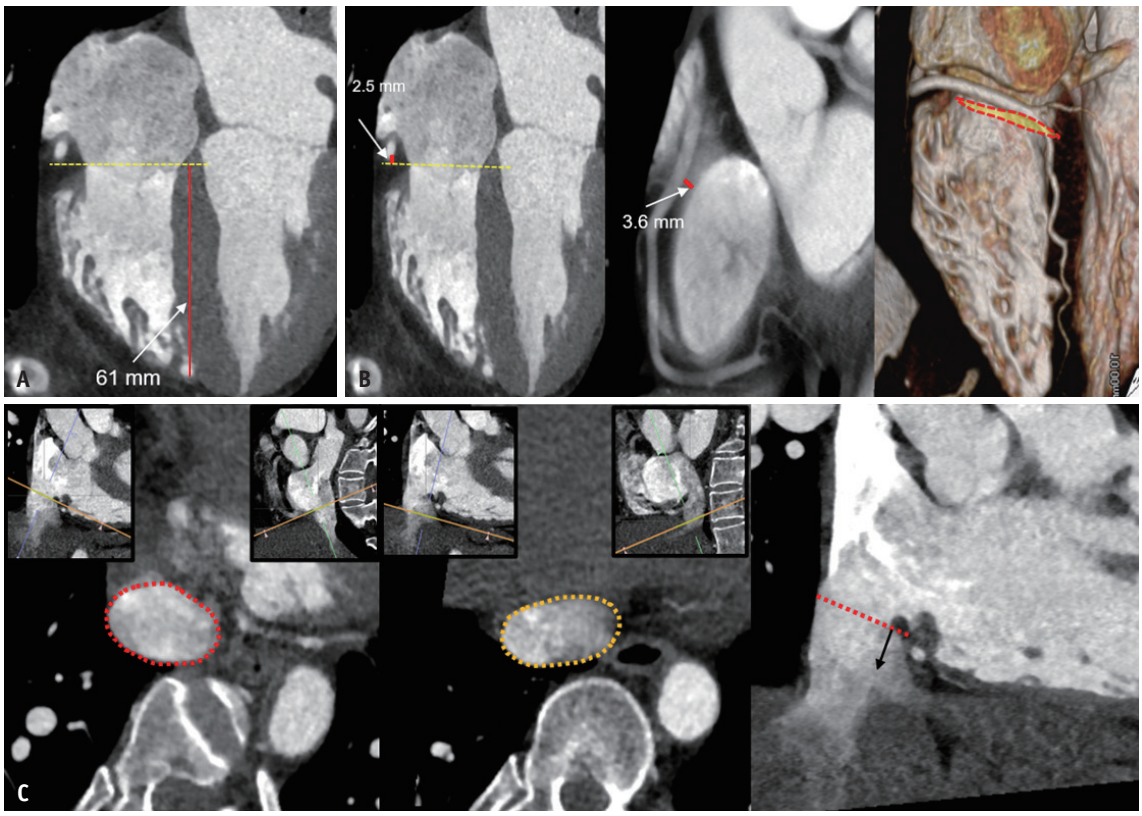

Fig. 14. Multiplanar reformation of cardiac CT for planning of transcatheter tricuspid valve therapy.
A. The distance from the tricuspid annulus to the right ventricular apex was measured to anchor the coaptation device. **B.** The distance between the RCA and tricuspid annulus was evaluated to select candidates for transcatheter tricuspid annuloplasty or transcatheter tricuspid valve replacement to prevent impingement of the RCA. The volume-rendered image can be helpful to determine the overall course of the RCA and its relationship with the tricuspid annulus (red-dotted area). **C.** The dimension of the inferior vena cava was measured for heterotopic caval valve implantation, with the measurement performed at the cavoatrial junction (red-dotted area and red-dotted line) and the 1st hepatic vein level (yellow-dotted area) on the multiplanar reconstructed images. The distance from the cavoatrial junction to the 1st hepatic vein (arrow) was also measured to prevent obstruction of the hepatic vein by the implanted valve. RCA = right coronary artery

useful.

3) Dimensions of caval veins: the dimensions of the inferior vena cava should be measured at the levels of the cavoatrial junction and the first hepatic vein for caval valve implantation. Additionally, the distance between the cavoatrial junction and the superior hepatic vein should be measured to prevent obstruction of the hepatic vein during valve implantation. The diameter of the superior vena cava valve was measured at the superior cavoatrial junction.

Postoperative Findings after Surgical Tricuspid Valve Replacement

Prosthetic Valve Thrombosis

Although prosthetic valve thrombosis is a rare complication, it can be fatal when not properly treated [49]. The incidence of prosthetic valve thrombosis in the tricuspid valve is up to 4.55% [50], whereas it is 0.55% in the aortic or mitral valve positions [51]. In general, bioprosthetic valve thrombosis occurs within 1–2 years after valve implantation in patients with risk factors of paroxysmal atrial fibrillation or a hypercoagulable state, such as recent withdrawal of oral anticoagulation or a subtherapeutic prothrombin time [52]. The elevated incidence of tricuspid valve thrombosis is thought to result from lower pressure on the right side of the heart across the prosthetic valve compared to that on the left side of the heart. Moreover, pulmonary hypertension can cause endothelial injury in the right atrium and ventricle, subsequently increasing the susceptibility to thrombus formation [49].

Usually, an initial diagnosis of prosthetic valve dysfunction is made using TTE or transesophageal echocardiography. Doppler parameters of a continuous wave with an emptying velocity > 1.7 m/s, a mean gradient > 6 mm Hg, or a pressure half-time > 230 ms suggest obstruction of the prosthetic tricuspid valve [53]. However, echocardiography

https://doi.org/10.3348/kjr.2020.1507

Korean Journal of Radiology
KJR

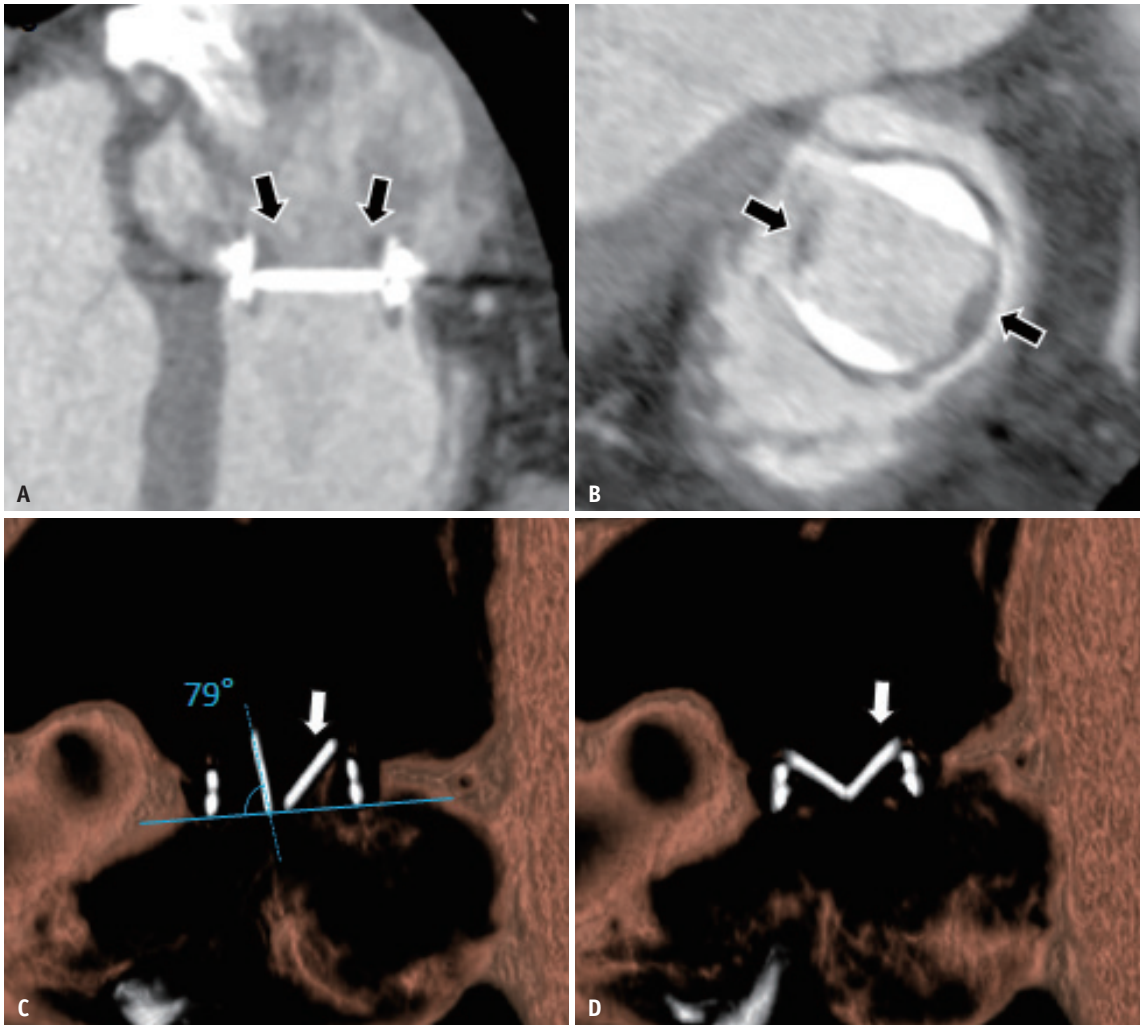

Fig. 15. Mechanical valve thrombosis. A 35-year-old male underwent tricuspid valve replacement with an On-X 31/33 mm. **A, B.** On cardiac CT acquired 6 years after the operation, low attenuating soft tissues (40–60 Hounsfield units) can be seen attached along the inner lumen of the prosthetic mitral valve (black arrows). **C, D.** An immobile posterior leaflet (white arrows) is observable on the volume-rendered profile view images during diastolic and systolic phases. The motion of the anterior leaflet was normal, with an opening angle of 79° being within the normal range. Supplementary Video 1 also demonstrates the immobile posterior leaflet on volume-rendered multiphase cardiac CT images.

has limited utility in the evaluation of leaflet motion due to acoustic shadowing and artifacts generated by the mechanical valve [49]. Cardiac CT has a complementary role in the assessment of prosthetic valve dysfunction by identifying thrombus formation and leaflet motion (Fig. 15) and distinguishing thrombus from pannus [54,55].

Subprosthetic Pannus Formation

Pannus is one of the main causes of prosthetic valve obstruction, with valve thrombosis restricting leaflet motion [56]. Pannus is an overgrowth of fibroblastic tissue with inflammatory cells and intervening capillary vessels in the periannular region [57]. Although it is considered a normal endocardial healing process after surgery, protrusion into the valve orifice can cause flow disturbance and consequent valve stenosis. The incidence of prosthetic valve obstruction by pannus accounts for 6.3% of left-sided prosthetic valve obstruction [58]; however, its incidence in prosthetic valves in the tricuspid position is unclear. Distinguishing pannus from valve thrombosis is crucial because of the different treatment options for the two conditions. According to the anatomical position, the pannus is usually located in the subvalvular area of the prosthetic valve ring, as a curved lesion along the valvular ring (Fig. 16). Conversely, thrombosis can be located both in the supra- and subvalvular areas, attaching to the leaflet and hinge point, and appears as an irregular hypodense mass [59]. HU measurement on cardiac CT can

 https://doi.org/10.3348/kjr.2020.1507

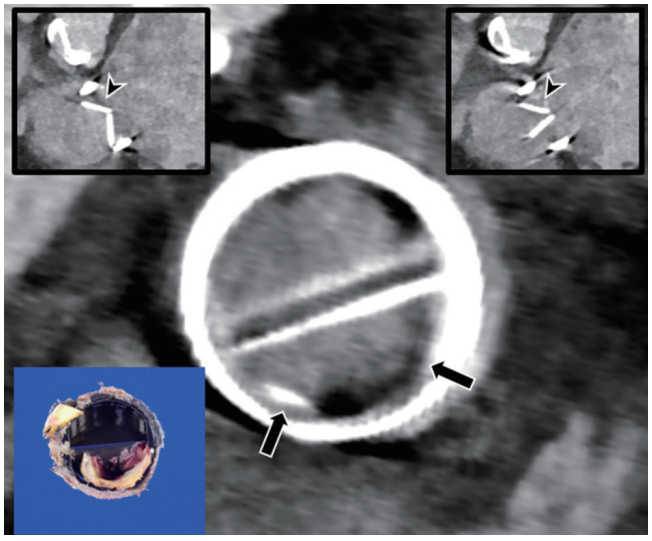

Fig. 16. Subprosthetic pannus formation. A 48-year-old female underwent tricuspid valve replacement with a CarboMedics 29 mm. Cardiac CT performed 15 years after the operation revealed a subvalvular curvilinear soft tissue lesion with calcifications. The soft tissue lesion showed attenuation of 145 Hounsfield units, suggesting pannus formation rather than thrombus (arrows). The anterior leaflet of the prosthetic valve was immobilized (arrowheads on two top boxes). The surgical specimen (left lower box) revealed fibrotic soft tissue corresponding to the CT findings.

help differentiate between pannus and thrombosis, with a cut-off > 145 HU predicting pannus with a sensitivity of 88% and specificity of 95% [60]. Because of its position, the mitral valve has a higher risk for pannus formation than the aortic valve, but is less commonly associated with valve obstruction than the aortic valve [61]. This may be attributable to the large annular size and lower turbulent flow in the mitral valve compared to the aortic valve [62]. Current investigations are insufficient to evaluate the complications of prosthetic tricuspid valves, such as pannus or thrombus, and future investigations are needed for clarification.

Prosthetic Valve Opening

Prosthetic valve thrombosis and pannus formation are the two main causes of prosthetic valve obstruction, and occur due to the restriction of leaflet motion [56]. ECG-gated cardiac CT can provide information on mechanical valve obstruction, enabling the evaluation of valves with nearly motion-free images, which can be reconstructed in any plane. The opening and closing angles are measured in the "in profile" projection (the view with beams parallel to both planes of the valve ring and tilting of the disc axis) and "en face" projection (view with beams parallel to the outflow tract of the valve), similar to the procedure in fluoroscopy (Fig. 16) [63]. A 3D volume-rendered image can be generated to demonstrate the motion of the prosthetic leaflets (Supplementary Movie 1). The opening angle is measured as the distance between the valve ring and the leaflets when fully opened. The normal range of the opening angle is 60°–80° for tilting disc valves and 73°–90° for bi-leaflet valves [63].

CONCLUSION

Cardiac CT and MRI can provide accurate and detailed depictions of the anatomy of the tricuspid valve and functional assessment of the RV and TR. Given the increasing number of elderly patients with comorbidities precluding surgical treatment of TR, transcatheter treatment options have emerged and are being investigated in clinical trials. To determine the treatment options for TR, a comprehensive and accurate anatomic and functional assessment by radiologists is important to facilitate appropriate patient selection and procedure guidance.

Supplement

The Supplement is available with this article at https://doi.org/10.3348/kjr.2020.1507.

Supplementary Movie Legends

Movie 1. A 35-year-old male underwent tricuspid valve replacement with an On-X 31/33 mm prosthetic heart valve. The 3D volume rendered image (first scene) intuitively shows the immobile posterior leaflet against the anterior leaflet showing normal motion. The reformatted multiplanar image (second scene) also shows the immobile posterior leaflet in both profile and en-face views.

Conflicts of Interest

The authors have no potential conflicts of interest to disclose.

Author Contributions

Conceptualization: all authors. Data curation: all authors. Supervision: Hyun Jung Koo, Dong Hyun Yang. Writing—original draft: Yura Ahn, Hyun Jung Koo, Dong Hyun Yang. Writing—review & editing: all authors.

Korean Journal of Radiology
KJR

ORCID iDs
Yura Ahn
https://orcid.org/0000-0002-9188-1186
Hyun Jung Koo
https://orcid.org/0000-0001-5640-3835
Joon-Won Kang
https://orcid.org/0000-0001-6478-0390
Dong Hyun Yang
https://orcid.org/0000-0001-5477-558X

REFERENCES

1. Koelling TM, Aaronson KD, Cody RJ, Bach DS, Armstrong WF. Prognostic significance of mitral regurgitation and tricuspid regurgitation in patients with left ventricular systolic dysfunction. *Am Heart J* 2002;144:524-529
2. Nath J, Foster E, Heidenreich PA. Impact of tricuspid regurgitation on long-term survival. *J Am Coll Cardiol* 2004;43:405-409
3. Kuriyama K, Gamsu G, Stern RG, Cann CE, Herfkens RJ, Brundage BH. CT-determined pulmonary artery diameters in predicting pulmonary hypertension. *Invest Radiol* 1984;19:16-22
4. Raman SV, Shah M, McCarthy B, Garcia A, Ferketich AK. Multi-detector row cardiac computed tomography accurately quantifies right and left ventricular size and function compared with cardiac magnetic resonance. *Am Heart J* 2006;151:736-744
5. Saremi F, Hassani C, Millan-Nunez V, Sánchez-Quintana D. Imaging evaluation of tricuspid valve: analysis of morphology and function with CT and MRI. *AJR Am J Roentgenol* 2015;204:W531-W542
6. Anderson RH, Ho SY, Becker AE. Anatomy of the human atrioventricular junctions revisited. *Anat Rec* 2000;260:81-91
7. Dahou A, Levin D, Reisman M, Hahn RT. Anatomy and physiology of the tricuspid valve. *JACC Cardiovasc Imaging* 2019;12:458-468
8. Fukuda S, Saracino G, Matsumura Y, Daimon M, Tran H, Greenberg NL, et al. Three-dimensional geometry of the tricuspid annulus in healthy subjects and in patients with functional tricuspid regurgitation: a real-time, 3-dimensional echocardiographic study. *Circulation* 2006;114:I492-I498
9. Kwan J, Kim GC, Jeon MJ, Kim DH, Shiota T, Thomas JD, et al. 3D geometry of a normal tricuspid annulus during systole: a comparison study with the mitral annulus using real-time 3D echocardiography. *Eur J Echocardiogr* 2007;8:375-383
10. Faletra FF, Leo LA, Paiocchi VL, Schlossbauer SA, Borruso MG, Pedrazzini G, et al. Imaging-based tricuspid valve anatomy by computed tomography, magnetic resonance imaging, two and three-dimensional echocardiography: correlation with anatomic specimen. *Eur Heart J Cardiovasc Imaging* 2019;20:1-13
11. Saremi F, Hassani C, Sánchez-Quintana D. Septal atrioventricular junction region: comprehensive imaging in adults. *Radiographics* 2016;36:1966-1986
12. Saremi F, Sánchez-Quintana D, Mori S, Muresian H, Spicer DE, Hassani C, et al. Fibrous skeleton of the heart: anatomic overview and evaluation of pathologic conditions with CT and MR imaging. *Radiographics* 2017;37:1330-1351
13. Asmarats L, Puri R, Latib A, Navia JL, Rodés-Cabau J. Transcatheter tricuspid valve interventions: landscape, challenges, and future directions. *J Am Coll Cardiol* 2018;71:2935-2956
14. Dreyfus GD, Martin RP, Chan KM, Dulguerov F, Alexandrescu C. Functional tricuspid regurgitation: a need to revise our understanding. *J Am Coll Cardiol* 2015;65:2331-2336
15. Johnson PT, Pannu HK, Fishman EK. IV contrast infusion for coronary artery CT angiography: literature review and results of a nationwide survey. *AJR Am J Roentgenol* 2009;192:W214-W221
16. Saremi F, Kang J, Rahmanuddin S, Shavelle D. Assessment of post-atrial switch baffle integrity using a modified dual extremity injection cardiac computed tomography angiography technique. *Int J Cardiol* 2013;162:e25-e27
17. Khalique OK, Cavalcante JL, Shah D, Guta AC, Zhan Y, Piazza N, et al. Multimodality imaging of the tricuspid valve and right heart anatomy. *JACC Cardiovasc Imaging* 2019;12:516-531
18. Shah S, Jenkins T, Markowitz A, Gilkeson R, Rajiah P. Multimodal imaging of the tricuspid valve: normal appearance and pathological entities. *Insights Imaging* 2016;7:649-667
19. Machida H, Tanaka I, Fukui R, Shen Y, Ishikawa T, Tate E, et al. Current and novel imaging techniques in coronary CT. *Radiographics* 2015;35:991-1010
20. Kang EJ. Clinical applications of wide-detector CT scanners for cardiothoracic imaging: an update. *Korean J Radiol* 2019;20:1583-1596
21. Naoum C, Blanke P, Leipsic J. Iterative reconstruction in cardiac CT. *J Cardiovasc Comput Tomogr* 2015;9:255-263
22. Habets J, Symersky P, de Mol BA, Mali WP, Leiner T, Budde RP. A novel iterative reconstruction algorithm allows reduced dose multidetector-row CT imaging of mechanical prosthetic heart valves. *Int J Cardiovasc Imaging* 2012;28:1567-1575
23. Tei C, Pilgrim JP, Shah PM, Ormiston JA, Wong M. The tricuspid valve annulus: study of size and motion in normal subjects and in patients with tricuspid regurgitation. *Circulation* 1982;66:665-671
24. Dwivedi G, Mahadevan G, Jimenez D, Frenneaux M, Steeds RP. Reference values for mitral and tricuspid annular dimensions using two-dimensional echocardiography. *Echo Res Pract* 2014;1:43-50
25. Badano LP, Muraru D, Enriquez-Sarano M. Assessment of functional tricuspid regurgitation. *Eur Heart J* 2013;34:1875-1885
26. Ton-Nu TT, Levine RA, Handschumacher MD, Dorer DJ, Yosefy C, Fan D, et al. Geometric determinants of functional tricuspid regurgitation: insights from 3-dimensional echocardiography.

 https://doi.org/10.3348/kjr.2020.1507

Circulation 2006;114:143-149
27. Dupont MV, Drăgean CA, Coche EE. Right ventricle function assessment by MDCT. *AJR Am J Roentgenol* 2011;196:77-86
28. Castañer E, Gallardo X, Ballesteros E, Andreu M, Pallardó Y, Mata JM, et al. CT diagnosis of chronic pulmonary thromboembolism. *Radiographics* 2009;29:31-50
29. Kawel-Boehm N, Maceira A, Valsangiacomo-Buechel ER, Vogel-Claussen J, Turkbey EB, Williams R, et al. Normal values for cardiovascular magnetic resonance in adults and children. *J Cardiovasc Magn Reson* 2015;17:29
30. Stojanovska J, Prasitdumrong H, Patel S, Sundaram B, Gross BH, Yilmaz ZN, et al. Reference absolute and indexed values for left and right ventricular volume, function and mass from cardiac computed tomography. *J Med Imaging Radiat Oncol* 2014;58:547-558
31. Rana BS, Robinson S, Francis R, Toshner M, Swaans MJ, Agarwal S, et al. Tricuspid regurgitation and the right ventricle in risk stratification and timing of intervention. *Echo Res Pract* 2019;6:R25-R39
32. Schulz-Menger J, Bluemke DA, Bremerich J, Flamm SD, Fogel MA, Friedrich MG, et al. Standardized image interpretation and post processing in cardiovascular magnetic resonance: Society for Cardiovascular Magnetic Resonance (SCMR) board of trustees task force on standardized post processing. *J Cardiovasc Magn Reson* 2020;22:19
33. Foppa M, Arora G, Gona P, Ashrafi A, Salton CJ, Yeon SB, et al. Right ventricular volumes and systolic function by cardiac magnetic resonance and the impact of sex, age, and obesity in a longitudinally followed cohort free of pulmonary and cardiovascular disease: the Framingham Heart Study. *Circ Cardiovasc Imaging* 2016;9:e003810
34. Zoghbi WA, Adams D, Bonow RO, Enriquez-Sarano M, Foster E, Grayburn PA, et al. Recommendations for noninvasive evaluation of native valvular regurgitation: a report from the American Society of Echocardiography developed in collaboration with the Society for Cardiovascular Magnetic Resonance. *J Am Soc Echocardiogr* 2017;30:303-371
35. Hahn RT, Thomas JD, Khalique OK, Cavalcante JL, Praz F, Zoghbi WA. Imaging assessment of tricuspid regurgitation severity. *JACC Cardiovasc Imaging* 2019;12:469-490
36. Kabasawa M, Kohno H, Ishizaka T, Ishida K, Funabashi N, Kataoka A, et al. Assessment of functional tricuspid regurgitation using 320-detector-row multislice computed tomography: risk factor analysis for recurrent regurgitation after tricuspid annuloplasty. *J Thorac Cardiovasc Surg* 2014;147:312-320
37. Kim H, Kim IC, Yoon HJ, Park HS, Cho YK, Nam CW, et al. Prognostic usefulness of tricuspid annular diameter for cardiovascular events in patients with tricuspid regurgitation of moderate to severe degree. *Am J Cardiol* 2018;121:1343-1350
38. Fukuda S, Song JM, Gillinov AM, McCarthy PM, Daimon M, Kongsaerepong V, et al. Tricuspid valve tethering predicts residual tricuspid regurgitation after tricuspid annuloplasty. *Circulation* 2005;111:975-979
39. Kramer CM, Barkhausen J, Bucciarelli-Ducci C, Flamm SD, Kim RJ, Nagel E. Standardized cardiovascular magnetic resonance imaging (CMR) protocols: 2020 update. *J Cardiovasc Magn Reson* 2020;22:17
40. Lee JW, Hur JH, Yang DH, Lee BY, Im DJ, Hong SJ, et al. Guidelines for cardiovascular magnetic resonance imaging from the Korean Society of Cardiovascular Imaging—Part 2: interpretation of cine, flow, and angiography data. *Korean J Radiol* 2019;20:1477-1490
41. Suzuki J, Caputo GR, Kondo C, Higgins CB. Cine MR imaging of valvular heart disease: display and imaging parameters affect the size of the signal void caused by valvular regurgitation. *AJR Am J Roentgenol* 1990;155:723-727
42. Jun H, Park EA, Bahn YE, Lee W, Kim HK, Chung JW. Quantification of tricuspid regurgitation using two-dimensional velocity encoding cine: optimal plane and reproducibility. *Int J Cardiovasc Imaging* 2015;31:233-240
43. Fender EA, Zack CJ, Nishimura RA. Isolated tricuspid regurgitation: outcomes and therapeutic interventions. *Heart* 2018;104:798-806
44. Rodés-Cabau J, Taramasso M, O'Gara PT. Diagnosis and treatment of tricuspid valve disease: current and future perspectives. *Lancet* 2016;388:2431-2442
45. Baumgartner H, Falk V, Bax JJ, De Bonis M, Hamm C, Holm PJ, et al. 2017 ESC/EACTS guidelines for the management of valvular heart disease. *Eur Heart J* 2017;38:2739-2791
46. Rodés-Cabau J, Hahn RT, Latib A, Laule M, Lauten A, Maisano F, et al. Transcatheter therapies for treating tricuspid regurgitation. *J Am Coll Cardiol* 2016;67:1829-1845
47. Wang DD, Lee JC, O'Neill BP, O'Neill WW. Multimodality imaging of the tricuspid valve for assessment and guidance of transcatheter repair. *Interv Cardiol Clin* 2018;7:379-386
48. van Rosendael PJ, Kamperidis V, Kong WK, van Rosendael AR, van der Kley F, Ajmone Marsan N, et al. Computed tomography for planning transcatheter tricuspid valve therapy. *Eur Heart J* 2017;38:665-674
49. Zaghloul A, Iorgoveanu C, Desai A, Silkowski M, Balakumaran K. Prosthetic tricuspid valve thrombosis. *Cureus* 2018;10:e2928
50. Rizzoli G, Vendramin I, Nesseris G, Bottio T, Guglielmi C, Schiavon L. Biological or mechanical prostheses in tricuspid position? A meta-analysis of intra-institutional results. *Ann Thorac Surg* 2004;77:1607-1614
51. Butany J, Ahluwalia MS, Munroe C, Fayet C, Ahn C, Blit P, et al. Mechanical heart valve prostheses: identification and evaluation. *Cardiovasc Pathol* 2003;12:322-344
52. Puri R, Auffret V, Rodés-Cabau J. Bioprosthetic valve thrombosis. *J Am Coll Cardiol* 2017;69:2193-2211
53. Zoghbi WA, Chambers JB, Dumesnil JG, Foster E, Gottdiener JS, Grayburn PA, et al. Recommendations for evaluation of prosthetic valves with echocardiography and doppler ultrasound: a report from the American Society of Echocardiography's guidelines and Standards Committee and

https://doi.org/10.3348/kjr.2020.1507

the Task Force on Prosthetic Valves, developed in conjunction with the American College of Cardiology Cardiovascular Imaging Committee, Cardiac Imaging Committee of the American Heart Association, the European Association of Echocardiography, a registered branch of the European Society of Cardiology, the Japanese Society of Echocardiography and the Canadian Society of Echocardiography, endorsed by the American College of Cardiology Foundation, American Heart Association, European Association of Echocardiography, a registered branch of the European Society of Cardiology, the Japanese Society of Echocardiography, and Canadian Society of Echocardiography. *J Am Soc Echocardiogr* 2009;22:975-1014
54. Teshima H, Hayashida N, Fukunaga S, Tayama E, Kawara T, Aoyagi S, et al. Usefulness of a multidetector-row computed tomography scanner for detecting pannus formation. *Ann Thorac Surg* 2004;77:523-526
55. Habets J, Symersky P, van Herwerden LA, de Mol BA, Spijkerboer AM, Mali WP, et al. Prosthetic heart valve assessment with multidetector-row CT: imaging characteristics of 91 valves in 83 patients. *Eur Radiol* 2011;21:1390-1396
56. Salamon J, Munoz-Mendoza J, Liebelt JJ, Taub CC. Mechanical valve obstruction: review of diagnostic and treatment strategies. *World J Cardiol* 2015;7:875-881
57. Teshima H, Hayashida N, Yano H, Nishimi M, Tayama E, Fukunaga S, et al. Obstruction of St Jude Medical valves in the aortic position: histology and immunohistochemistry of pannus. *J Thorac Cardiovasc Surg* 2003;126:401-407
58. Deviri E, Sareli P, Wisenbaugh T, Cronje SL. Obstruction of mechanical heart valve prostheses: clinical aspects and surgical management. *J Am Coll Cardiol* 1991;17:646-650
59. Tanis W, Habets J, van den Brink RB, Symersky P, Budde RP, Chamuleau SA. Differentiation of thrombus from pannus as the cause of acquired mechanical prosthetic heart valve obstruction by non-invasive imaging: a review of the literature. *Eur Heart J Cardiovasc Imaging* 2013;15:119-129
60. Gündüz S, Özkan M, Kalçik M, Gürsoy OM, Astarcioğlu MA, Karakoyun S, et al. Sixty-four-section cardiac computed tomography in mechanical prosthetic heart valve dysfunction: thrombus or pannus. *Circ Cardiovasc Imaging* 2015;8:e003246
61. Rajiah P, Moore A, Saboo S, Goerne H, Ranganath P, MacNamara J, et al. Multimodality imaging of complications of cardiac valve surgeries. *Radiographics* 2019;39:932-956
62. Chang S, Suh YJ, Han K, Kim JY, Kim YJ, Chang BC, et al. The clinical significance of perivalvular pannus in prosthetic mitral valves: can cardiac CT be helpful? *Int J Cardiol* 2017;249:344-348
63. Lancellotti P, Pibarot P, Chambers J, Edvardsen T, Delgado V, Dulgheru R, et al. Recommendations for the imaging assessment of prosthetic heart valves: a report from the European Association of Cardiovascular Imaging endorsed by the Chinese Society of Echocardiography, the Inter-American Society of Echocardiography, and the Brazilian Department of Cardiovascular Imaging. *Eur Heart J Cardiovasc Imaging* 2016;17:589-590

 https://doi.org/10.3348/kjr.2020.1507